Influence of Morphology on the Dynamic Mechanical Properties of Hydrogenated Acrylonitrile Butadiene Elastomer/Coagent Nanodispersions

Blaž Likozar, Matjaž Krajnc

Faculty of Chemistry and Chemical Technology, University of Ljubljana, Aškerčeva Cesta 5, 1000 Ljubljana, Slovenia

Received 11 July 2007; accepted 2 November 2007
DOI 10.1002/app.28525
Published online 18 June 2008 in Wiley InterScience (www.interscience.wiley.com).

ABSTRACT: Coagents are vinyl monomers that react with free radicals formed by peroxide dissociation and are either grafted to elastomer chains or homopolymerized within a segregated phase to form a crosslinked network. The initial phase distribution within the elastomer matrix is of great importance for the final user properties of a composite material. In this study, the morphology of blends of each of three different coagents, that is, zinc dimethacrylate (ZDMA), *N,N′-m*-phenylene dimaleimide (HVA-2), and trimethylolpropane trimethacrylate (TMPTMA) on a reinforcing substrate with dicumyl peroxide and hydrogenated acrylonitrile butadiene elastomer after processing was investigated with scanning electron microscopy. The morphology that evolved during processing was then compared to the results obtained from dynamic mechanical analysis (DMA) of the blends. Dynamic mechanical properties were modeled with a continuous relaxation distribution function, the Williams–Landel–Ferry equation, and the modified Guth–Gold equation. In the case of ZDMA and TMPTMA, a microphase and a nanophase evolved during processing, whereas the HVA-2 phase in the blends remained well segregated. The volume fraction of the particles under 100 nm in ZDMA and TMPTMA blends ranged from 79 to 89%. The DMA results revealed the reinforcing effect of ZDMA and TMPTMA during the glass-transition and in the plateau region, whereas HVA-2 exhibited plasticizer-like behavior. © 2008 Wiley Periodicals, Inc. J Appl Polym Sci 110: 183–195, 2008

Key words: elastomers; mechanical properties; morphology; nanocomposites

INTRODUCTION

The use of coagents in conjunction with peroxides to cure elastomers has been common practice in the rubber industry for many years. Coagents are typically multifunctional vinyl monomers that are highly reactive toward free radicals and readily graft to elastomer chains to form a complex crosslinked network. Because all common coagents contain terminal unsaturations, it can be concluded that addition/polymerization is the principal mechanism by which they react in a compound.[1] This has been confirmed by studies that observed a loss of coagent unsaturation during peroxide curing.[1] These additives are used to improve the physical properties and processability of peroxide-cured elastomers. With peroxide-cured elastomers, they increase not only the crosslinking efficiency of the vulcanization process but the crosslink density as well.[2–5] The increase in the crosslink density is directly related to the coagent concentration and has a major impact on the mechanical and physical properties of the cured elastomer. The latter are also affected by the blend morphology because even if the initial mixing is adequate, a significant portion of the coagent can be anticipated to phase-separate into distinct domains.[6] It can be expected that this region will during crosslinking also eventually be covalently bonded to the surrounding elastomer matrix.[7] The balance of homopolymerization over polymer grafting depends on the concentration, polarity differences between the coagent and elastomer, and adequacy of mixing.[1] Some of the most common coagents in use today are esters of acrylic and methacrylic acid, *N,N′-m*-phenylene dimaleimide (HVA-2) and zinc dimethacrylate (ZDMA). Trimethylolpropane triacrylate (TMPTA), trimethylolpropane trimethacrylate (TMPTMA), and 1,3-butylene glycol dimethacrylate are typical examples of the acrylate and methacrylate ester class of coagents.

There are three possible types of elastomer/coagent blends. The first is the ordinary blend, which is prepared through the mixing of a coagent into an elastomer. The other two types are formed when a coagent on a reinforcing substrate is mixed

Correspondence to: M. Krajnc (matjaz.krajnc@fkkt.uni-lj.si).
Contract grant sponsor: Slovenian Ministry of Higher Education, Science and Technology; contract grant number: L2-6686.

into an elastomer or the coagent reinforces itself; this is the case of ZDMA. In the latter two cases, elastomer/coagent nanodispersions are formed, provided that the mixing is adequate. In this study, blends of coagents ZDMA, HVA-2, and TMPTMA on a reinforcing substrate and hydrogenated acrylonitrile butadiene elastomer (HNBR) were investigated.

ZDMA-loaded, peroxide-cured HNBR was found to possess high tensile strength.[8] Since then, several studies have been published on the topic of ZDMA's dramatic reinforcement of elastomers. Inoue[9] discussed the reaction-induced phase decomposition of ZDMA during peroxide curing with diene polymers. Ikeda and coworkers[6,10] studied and simulated the *in situ* copolymerization behavior of ZDMA in HNBR during peroxide crosslinking. Recently, Lu and coworkers[11,12] investigated the morphology and mechanical properties of ZDMA-reinforced HNBR. Although most of the articles cover ZDMA-reinforced HNBR, blends with other elastomers such as acrylonitrile butadiene elastomer,[11–14] styrene butadiene elastomer,[11,12] ethylene propylene diene elastomer,[11,12,15] ethylene propylene elastomer,[11,12] and poly(α-octene-*co*-ethylene) elastomer[11,12,16] have been examined as well.

The applicability of bismaleimides ranges from various resins such as epoxy/novolac[17] and diamine[18,19] to elastomers. In the latter case, HVA-2 is often used as a compatibilizer in blends. It influences the mechanical and morphological properties of blends and has been shown to effectively act as a multifunctional radical acceptor, promoting the combination of dissimilar polymer radicals and reducing interfacial tension.[20] The dimaleimide crosslinks are very stable upon the exposure of the blend to increased temperatures, and this makes it an attractive material for the dynamic crosslinking of various blends.[20] Hassan et al.[20] investigated the effect of HVA-2 on the mechanical and morphological properties of polypropylene/natural rubber/linear low-density polyethylene blends, whereas Inoue and Suzuki[21,22] in a series of articles examined polypropylene/ethylene propylene diene elastomer/HVA-2 blends.

The addition of TMPTMA during elastomer processing is used to improve miscibility. The polyfunctional monomer TMPTMA may reduce interfacial tension and increase the adhesion force between the polymer phases, allowing finer dispersions and a more stable morphology.[23] The compatibility of an elastomer blend can be affected by the species produced during TMPTMA's thermal oxidation. These advantages explain the fact that TMPTMA is widely employed and studied in many diverse fields of applications. Among others, its blends with polyethylene,[23–25] polypropylene,[23] poly(ethylene-*co*-vinylacetate),[24,26] ethylene propylene diene elastomer,[27] acrylonitrile butadiene elastomer,[28] poly(vinyl chloride),[2,5,7,29] and natural rubber[30] have been investigated in recent years. Besides in ordinarily peroxide-crosslinked polymers, its effect on structural modification is advantageous even in the case of electron-beam curing.[24,26–31]

In this study, the morphology of blends of coagents ZDMA, HVA-2, and TMPTMA on a reinforcing substrate and HNBR after processing was investigated. The morphology that evolved during processing was then linked to the material's dynamic mechanical properties before crosslinking. The Williams–Landel–Ferry (WLF) equation,[32] which is along with its equivalent, the Vogel–Fulcher–Tammann equation,[33] still one of the most frequently used relationships between shift factors and temperature for moderately wide temperature ranges,[34–36] was applied for the purpose of modeling the blends' frequency–temperature behavior. A continuous relaxation distribution function was adopted in the model for the neat elastomer, whereas the storage modulus (G') values of the reinforced compound were examined with a relationship taking into account the concentration of the reinforcing agent.

EXPERIMENTAL

The HNBR used in this study was Zetpol 2020L, produced by Zeon Chemicals (Bayport, TX), with a nominal density of 950 kg/m^3, 36.2% bound acrylonitrile, an iodine value of 28 mg/100 mg (91% saturation), and a Mooney viscosity (ML_{1+4}, 100°C) of 57.5. A number-average molecular weight of 7.72×10^4 g/mol and a weight-average molecular weight of 2.36×10^5 g/mol were determined by gel permeation chromatography. The number-average molecular weight and weight-average molecular weight determination was performed with a Waters 2690 (Milford, MA) (separations module) instrument with a refractive-index detector. Three Waters Styragel columns (300 × 4.6 mm) were used in series. The HNBR solutions were prepared in tetrahydrofuran, which was also used as a carrier solvent at a rate of 0.2 mL/min. The average molecular weights were calculated from molecular weight/retention time curves of polystyrene standards. The peroxide crosslinking agent was dicumyl peroxide (DCP) from Aldrich (St. Louis, MO) (98% pure), with a molecular mass of 270.4 g/mol and a density of 1560 kg/m^3. The coagents were ZDMA from Aldrich (99% pure), with a molecular mass of 235.5 g/mol and a density of 1485 kg/m^3, TMPTMA absorbed on Microcel E (calcium silicate) from Akrochem (Akron, OH) (75% active ingredient), with the industrial name Akrosorb 29126, a molecular mass of 338.3 g/mol, and a density of 1370 kg/m^3, and HVA-2 from Sartomer (Exton, PA) (100% pure), with the industrial

TABLE I
Formulation of the Elastomer Compounds

	Compound weight (g)			
Ingredient	1	2, 3, 4	5, 6, 7	8, 9, 10
HNBR	50	50	50	50
DCP	0.764	0.764, 0.764, 0.764	0.764, 0.764, 0.764	0.764, 0.764, 0.764
ZDMA	—	0.791, 1.582, 3.165	—	—
TMPTMA	—	—	1.000, 2.000, 4.000	—
HVA-2	—	—	—	0.892, 1.784, 3.568

name SR525A, a molecular mass of 268.2 g/mol, and a density of 1440 kg/m^3.

All components in the formulation were stored at a low temperature. They were mixed into the elastomer on a Brabender (Duisburg, Germany) Plasti-Corder PLD-Type 651 instrument equipped with a W 50 C measuring mixer with the maximum torque of 100 Nm at 30°C. The temperature rose during mixing because of friction but never exceeded 110°C, so the extent of peroxide dissociation was minimized. Moreover, the measuring mixer was hermetically closed to prevent any loss of components due to evaporation. Mixing was performed for 15 min, whereas the coagents were added after 5 min and peroxide was added after 10 min. The formulation of the elastomer compounds is presented in Table I.

High-resolution liquid attached proton test (APT) carbon nuclear magnetic resonance (^{13}C-NMR) spectra were registered on a Varian Unity Inova 300 (Palo Alto, CA) spectrometer with a working frequency of 76.2 MHz with tubes 10 mm in diameter and under the following conditions: pulse angles of 90 and 180° according to the APT sequence and a digital resolution of 0.138 Hz/point corresponding to the spectral width of 18,000 Hz. A weighed portion of the samples was dissolved in deuterated chloroform ($CDCl_3$; 99.96%) containing tetramethylsilane (0.03%) as the internal reference (2 mL).

Samples for field emission scanning electron microscopy were cut from the compounds. Approximately 2-mm-thick samples were then exposed to carbon vapor for a sufficiently long time to achieve approximately 15-nm layer deposition. Micrographs were taken with field emission scanning electron microscopy (Supra 35 VP, Zeiss, Thornwood, NY) at 1–20 kV with different magnifications and contrasted with a quadrant backscattering detector. Images were processed with AnalySIS 5.0 (Soft Imaging System, Münster, Germany).

Dynamic mechanical properties were measured in the shear mode on a DMA861[e] instrument from Mettler–Toledo (Columbus, OH). The samples were prepared in a disc shape with a thickness between 1.1 and 2.1 mm and a diameter between 13.7 and 14.7 mm. Test measurements were performed for various samples with a thickness between 1 and 3 mm and a diameter between 10 and 15 mm to confirm that the sample's geometry had no effect on the measured properties. A linearity check was executed so that the measurements were performed within the linear viscoelastic regime, that is, within a 10-N force amplitude and a 10-μm displacement amplitude. Dynamic experiments were performed from −50 to 100°C with a constant heating rate (β) ranging between 1 and 5 K/min at constant frequencies between 0.01 and 100 Hz. All experiments were performed in a nitrogen atmosphere.

Differential scanning calorimetry (DSC) measurements were conducted on a DSC 821[e] instrument from Mettler–Toledo in a nitrogen atmosphere (50 mL/min). The samples were prepared by the weighing of 4–10 mg of the compound in 40-μL aluminum crucibles without a pin. The samples were first heated from 20 to 100°C to erase the samples' thermal history, then quenched to −50°C, and finally again heated to 100°C with constant heating and cooling rates of 10 K/min. Indium and zinc standards were applied for the temperature calibration and for the determination of the instrument time constant.

RESULTS AND DISCUSSION

If crosslinking agents such as peroxides or coagents themselves are susceptible to increased temperature, the crosslinking might occur even during blending. In such a case, reactive blending occurs, and the coagent either homopolymerizes within its phase or is grafted to the elastomer chains at the elastomer/coagent interface and in the diffusion layer. As the blending temperature was kept below 110°C, the extent of DCP decomposition was minimal.[37] The extent of any reactions whatsoever was examined with APT ^{13}C-NMR. The spectra for compounds 1, 4, 7, and 10 are presented in Figure 1.

The spectrum of the ZDMA blend is relatively similar to the one of the HNBR/DCP compound, except for the four peaks, which can be ascribed to ZDMA. Upon a review of the literature, no polymerized ZDMA spectra could be found to the best of

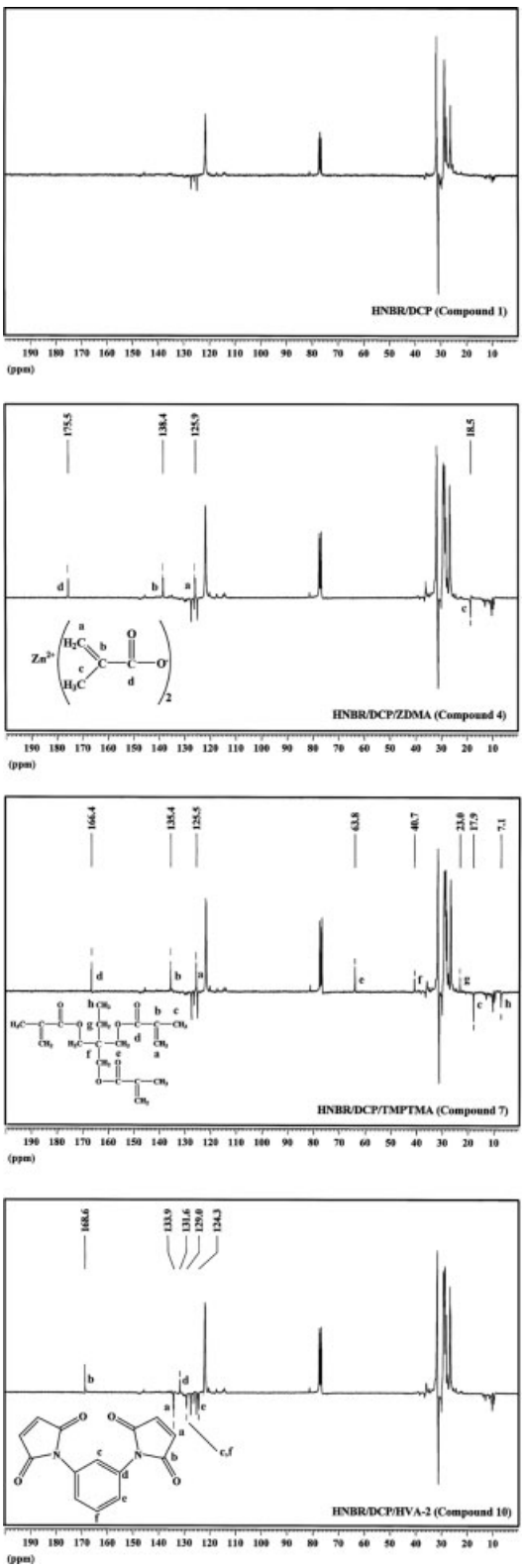

Figure 1 APT ^{13}C-NMR spectra of the ZDMA, TMPTMA, and HVA-2 blends.

our knowledge. The spectra were thus simulated with ACD/CNMR Predictor 10.0. Carbon atoms in polymerized ZDMA exhibit characteristic peaks between 20 and 25 ppm (carbon c, Fig. 1), 40 and 45 ppm (carbon b, Fig. 1), 45 and 50 ppm (carbon a, Fig. 1), and 180 and 185 ppm (carbon d, Fig. 1) for the head–tail configuration of the polymer and between 15 and 20 ppm (carbon c, Fig. 1), 45 and 50 ppm (carbon b, Fig. 1), 25 and 30 ppm (carbon a, Fig. 1), and 175 and 180 ppm (carbon d, Fig. 1) for the head–head configuration of the polymer. Because none of the characteristic peaks could be observed within some of these ranges (i.e., 40–50 ppm), we concluded that below 110°C, the homopolymerization's extent is rather small if not negligible.

The spectra for TMPTMA and HVA-2 were examined analogously. When polymerized, TMPTMA forms a crosslinked network because of its polyfunctionality, and the vinyl characteristic peak at 166 ppm decreases on account of the rising peak at about 175 ppm.[38] The latter cannot be seen in the TMPTMA blend spectrum. HVA-2 does not react either, because Grenier-Loustalot and Da Cunha[39] showed that during the polymerization of HVA-2, the maleimide carbonyl peak at 169 ppm gradually diminishes as the succinimide carbonyl peak at approximately 180 ppm increases. Alongside, the maleimide vinyl peak at 134 ppm decreases as the succinimide tertiary carbon peak at approximately 40 ppm appears. This, however, cannot be observed in Figure 1.

ZDMA, TMPTMA, and HVA-2 powders were prepared so that the majority of particles (>90%) had a relatively uniform maximal dimension between 1 and 2 μm before blend preparation. The particles tended to be rather irregular, whereas some could be considered spherical; Lu et al.[11] observed rodlike ZDMA particles. The ZDMA particle surface consisted of fibrillar structures, which were also observed by Lu et al. and were ascribed to the ZDMA microcrystals. On the other hand, the further enlargement of the observed TMPTMA and HVA-2 particles did not reveal any periodic pattern save for a certain degree of irregularity. Except for the latter, the surface of TMPTMA and HVA-2 particles appeared to be relatively smooth.

The morphology of the blends is presented in Figure 2. The morphology of the HNBR/DCP/ZDMA and HNBR/DCP/TMPTMA blends is biphasic in nature, with ZDMA and TMPTMA particles distributed in the HNBR matrix [Fig. 2(a,b)]. The presence of both microphase- and nanophase-separated morphology in the system indicates the foundation for the formation of interpenetrating polymer networks during crosslinking. This may lead to enhanced properties. Samui et al.[13] observed similar behavior of nitrile butadiene elastomer/zirconium tetramethacrylate blends. On the other hand, in the HNBR/DCP/HVA-2 blends, the coagent phase exhibits a lesser tendency to segregate and remains inhomogeneous even on a macroscale [Fig. 2(c)].

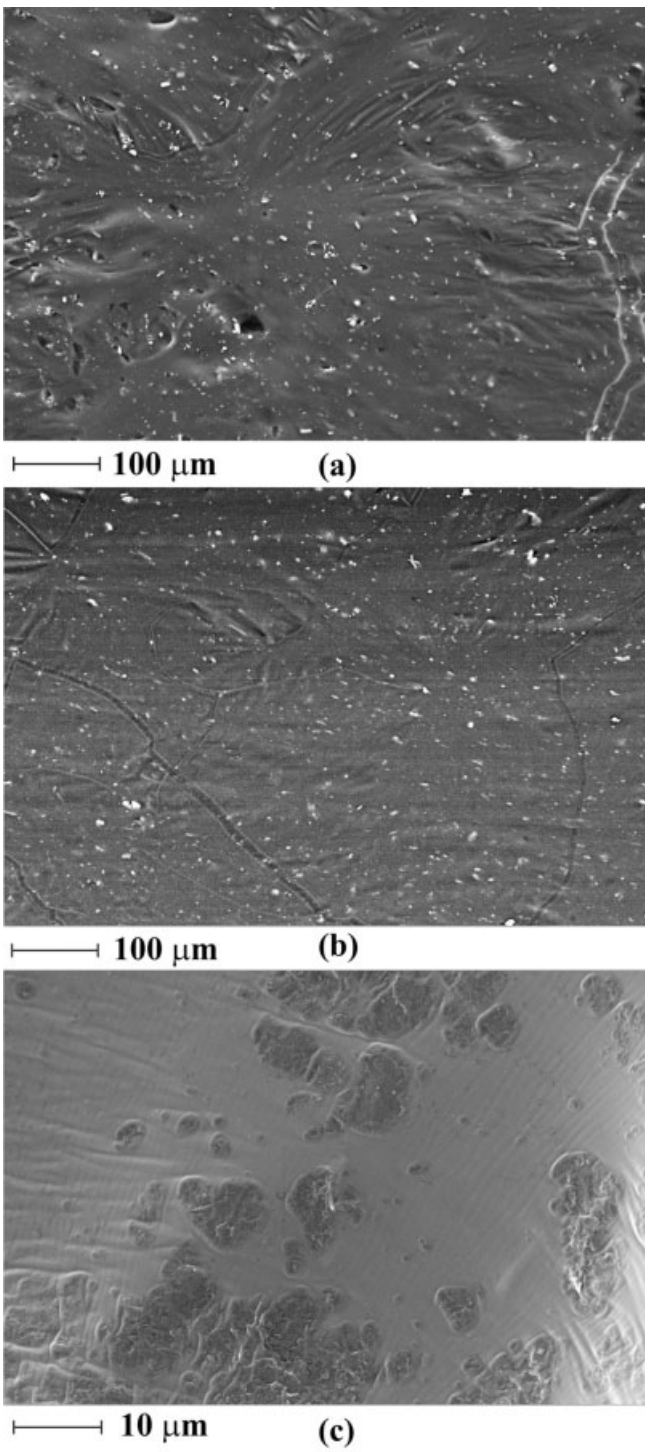

Figure 2 Scanning electron micrographs of (a) HNBR/DCP/ZDMA blend (compound 4), (b) HNBR/DCP/TMPTMA blend (compound 7), and (c) HNBR/DCP/HVA-2 blend (compound 10).

Because all three coagents (ZDMA, TMPTMA, and HVA-2) are highly polar, they are supposed to be similarly miscible with HNBR elastomer, the polarity of which arises from the acrylonitrile segments in the elastomer backbone. The effect of polarity differences between a coagent and the elastomer may not necessarily be considered crucial for the dispersion of the coagent in the rubber matrix, although the tendency of segregation of the HVA-2 phase in blends can be partially ascribed to the nonpolar phenyl group. The nonpolarity of the latter is inversely paralleled by the extremely polar character of the methacrylate ion in ZDMA. TMPTMA is less polar than ZDMA yet more polar than HVA-2, so the relatively good miscibility with the elastomer phase probably occurs because of the nature of the substrate, which is polar as well and indirectly causes matrix dispersion of substrate-diluted TMPTMA. In this case, the nature of the coagent itself may not be considered principally responsible for its miscibility.

The morphology of compounds 2–7 was examined statistically with a particle size threshold of 100 nm, whereas the coagent phase remained largely not segregated in compounds 8–10; this rendered the analysis meaningless. Several surfaces of the same compound were examined at different magnifications. The histograms in Figure 3 indicate that at the lower concentration of ZDMA in the compound, a greater number of particles under 1 μm are obtained. At higher concentrations, however, the two ZDMA phases become more distinct because the greatest fraction of the microphase is between 1 and 2 μm and the nanophase is under 100 nm. Lu et al.[11] also obtained micrometer-level dispersions of ZDMA in several elastomer matrices and observed that the dispersion level depends on the type of elastomer. During the mechanical mixing process of HNBR with ZDMA particles, the sizes of the particles of the latter decrease, but the reduction degree and the dispersion level of the compounds depend on the ZDMA loading.[11] If the distributions of particles' sizes are compared with respect to the equivalent circular diameter [d_E; Fig. 3(a–c)] and mean Feret diameter [d_F; Fig. 3(d–3f)], the conclusion can be made that the particles may be considered spherical because the distributions are relatively similar, regardless of the characteristic dimension. Histograms in Figure 4, however, indicate that in the TMPTMA compounds the greatest number of particles is below 1 μm. Only in compound 7 [Fig. 4(c)] does the hint of predominating microphase evolution become visible between 1 and 2 μm. This occurs in the case of TMPTMA at higher loadings than in the case of ZDMA. In the TMPTMA compounds, the coagent particles also tend to form a spherical shape, which may be seen upon a comparison of the distributions of d_E and d_F. For both ZDMA and TMPTMA blends, the observation can be made that the discrepancies from the spherical shape arise with the increasing coagent loading. In view of the fact that the micrographs were subjected to the statistical treatment with the particle size threshold of 100 nm,

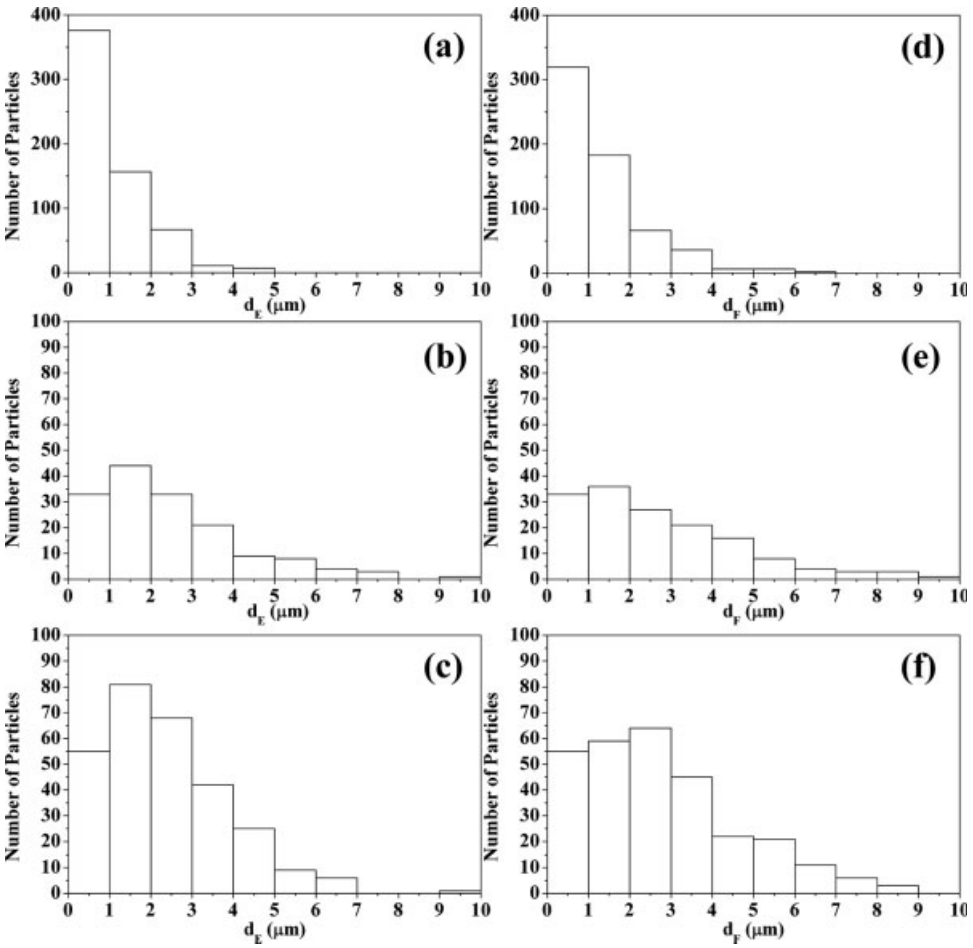

Figure 3 Distribution of particles larger than 100 nm in the HNBR/DCP/ZDMA blends: compounds (a) 2, (b) 3, (c) 4, (d) 2, (e) 3, and (f) 4 (the number of particles is normalized per area of the micrographs in Fig. 2).

the nanophase volume fraction normalized to the total coagent volume fraction can be calculated according to eq. (1), which takes into account the assumptions of relatively spherical particles, homogeneity, and isotropy of the compounds:

$$\varphi = 1 - \frac{\frac{\pi}{4}\sum_{i=1}^{I} d_{Ei}^2 \left(1 + \frac{w_{\mathrm{HNBR}}}{w_{\mathrm{Coagent}}}\frac{\rho_{\mathrm{Coagent}}}{\rho_{\mathrm{HNBR}}} + \frac{w_{\mathrm{DCP}}}{w_{\mathrm{Coagent}}}\frac{\rho_{\mathrm{Coagent}}}{\rho_{\mathrm{DCP}}}\right)}{A} \quad (1)$$

where φ represents the nanophase volume fraction, w is the weight fraction, ρ is the density, and A is the area of the micrograph subjected to the statistical treatment. The nanophase in the compounds consists of fibrillar dispersion structures with maximal Feret diameters lower than 100 nm, and this is likely related to the fibrillar structure at the ZDMA surface.[11] The nanophase fractions are presented in Table II. In both the ZDMA and TMPTMA blends, the fraction increases with the coagent concentration, yet it may be noted that the increase is not linear if the coagent loading is 2 or 4 times that of the one in compound 2 or 5 for ZDMA or TMPTMA, respectively. This implies that there is some boundary saturation of the elastomer phase with the nanophase, after which the evolution of the microphase becomes more explicit. Overall, the volume fraction of the nanophase is substantial in either the ZDMA or TMPTMA compounds. During mechanical mixing, a large number of microlevel particles were thus ground into smaller particles and even ultrafine particles whose sizes were nanolevel, and this led to the reduction in the dimensions and amounts of microlevel particles in HNBR.[11]

DSC thermograms in Figure 5 show that the incorporation of the reinforcing coagent influences the glass-transition behavior of HNBR. The glass-transition midpoint temperature (T_g) shifts toward higher temperatures as the amount of either ZDMA or TMPTMA in the compound is increased. The reason for the increase is that the mobility of HNBR chains is restricted. Analogous behavior was reported by Liu et al.[40] for nitrile butadiene elastomer/ZDMA/organomontmorillonite composites. The impact of the coagent in this case was much more intense because of the higher coagent loading and

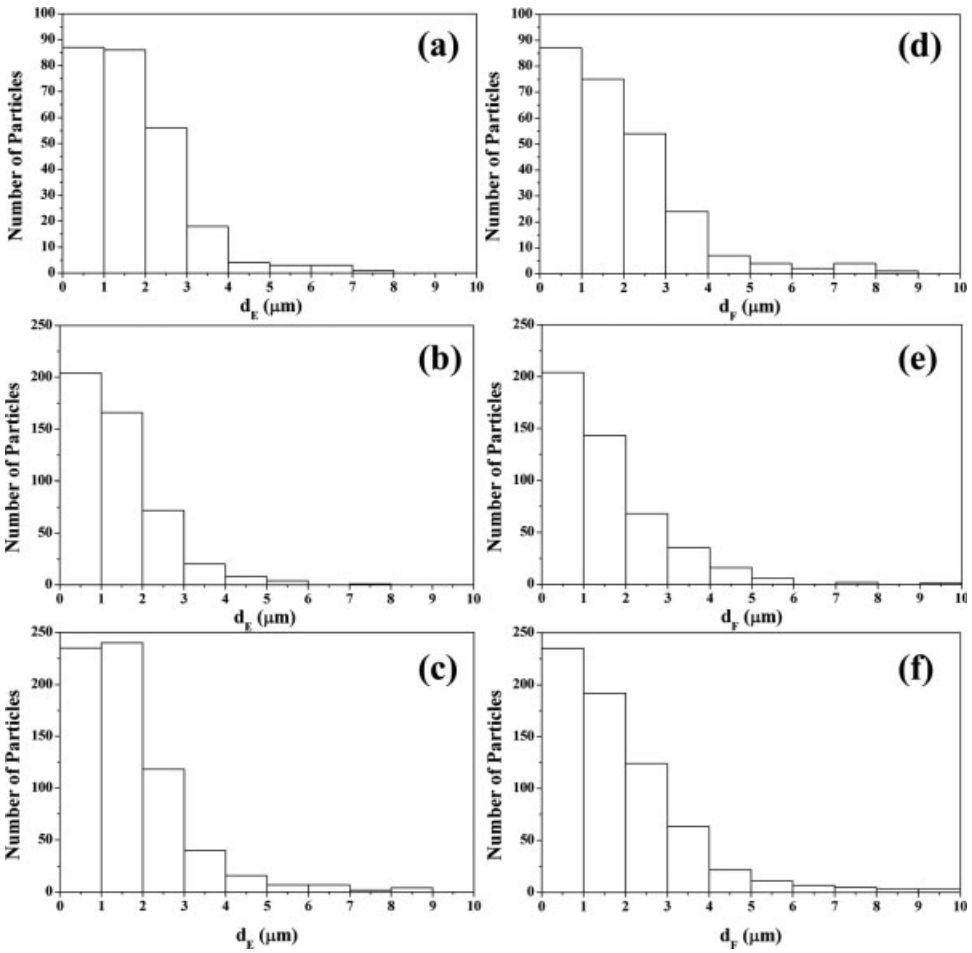

Figure 4 Distribution of particles larger than 100 nm in the HNBR/DCP/TMPTMA blends: compounds (a) 5, (b) 6, (c) 7, (d) 5, (e) 6, and (f) 7 (the number of particles is normalized per area of the micrographs in Fig. 2).

crosslinking before DSC studies. Upon the addition of HVA-2 to the compound, however, the effect of the coagent is the opposite, with a plasticizer-like behavior being exhibited. Altogether, the influence of all three coagents is rather limited.

G' and tan δ, presented in Figure 6 for compounds 1, 4, and 7, imply that ZDMA and TMPTMA exhibit the reinforcing effect of the HNBR matrix, which resembles the effects of fillers such as carbon black.[41] Usually, pure TMPTMA in compounds decreases T_g and functions as a plasticizer.[5] In our case, however, the reinforcing TMPTMA substrate was responsible for the opposite effect. Ikeda et al.[6] revealed that at greater ZDMA loadings, the latter can function as a plasticizer as well, and this was proved by dynamic mechanical analysis after the extraction of the unreacted ZDMA. Thus, the inversion of functionality apparently occurs, ZDMA serving as a reinforcing agent at lower concentrations and as a plasticizer at higher concentrations. Both ZDMA and TMPTMA have little effect on G' and tan δ in the initial plateau region, that is, the glassy state. It can be seen that neither ZDMA nor TMPTMA essentially shift the glass transition itself, as G' starts to decrease and tan δ reaches the maximum at relatively comparable temperatures. The DSC scans (Fig. 5) confirm these findings. The tan δ maximum decreases as the amount of the reinforcing coagent in the compound is increased. The higher the rubbery plateau modulus is after T_g, the larger the amount is of either ZDMA or TMPTMA in the compound. This can be ascribed to the fact that HNBR, occluded within the void of the reinforcing coagent aggregates but to an even greater extent adsorbed

TABLE II
Fraction of Particles Under 100 nm for the ZDMA and TMPTMA Compounds

Compound	Particles under 100 nm (vol %)
ZDMA (compound 2)	78.8
ZDMA (compound 3)	86.1
ZDMA (compound 4)	89.0
TMPTMA (compound 5)	80.7
TMPTMA (compound 6)	87.7
TMPTMA (compound 7)	88.5

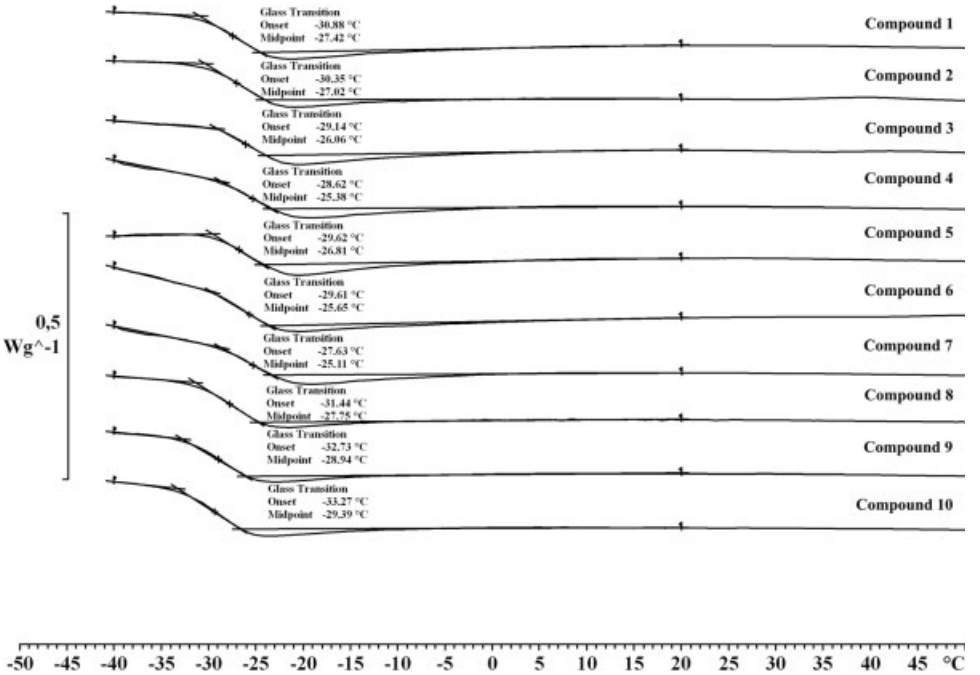

Figure 5 DSC thermograms for compounds 1–10.

onto the nanophase coagent surface, is not free to fully share in the microscopic deformation of a compound.[42] This immobilized elastomer may be identified with bound rubber. Because of their independent nature, the occluded elastomer and adsorbed elastomer can overlap each other and form a complicated interlinked system.[42] This hard immobilized elastomer fraction increases with both ZDMA and TMPTMA loading. Because the immobilized elastomer perturbs the relaxation responses of the matrix, diffused maxima in the tan δ values (which decrease progressively with the reinforcing coagent loading) at the glass–rubber transition region can be observed and may be attributed to the superposition of different relaxation processes.[41] G' then increases from the rubbery plateau, but the more gradually it does so, the greater the amount is of the reinforcing coagent. This happens because the structure ordering through the secondary bond crosslinking is hindered, the ZDMA and TMPTMA particles are percolated by the HNBR network, and crosslinking around these particles is not possible (Fig. 7). The term *crosslinking* refers exclusively to the occurrence of crosslinks due to secondary bonding and is not

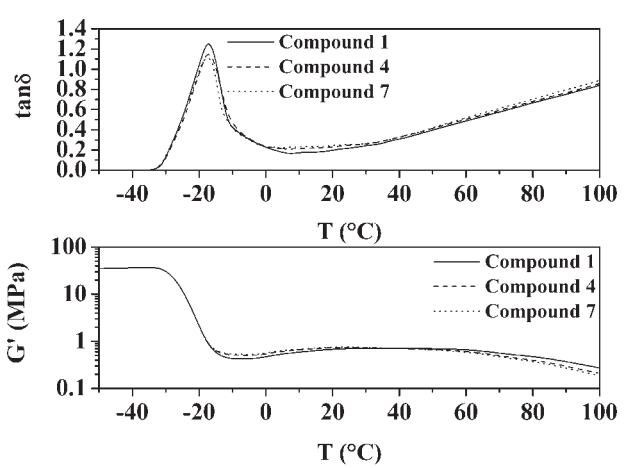

Figure 6 Variation of G' and tan δ with temperature (constant frequency = 1 Hz and β = 1 K/min) for compounds 1, 4, and 7.

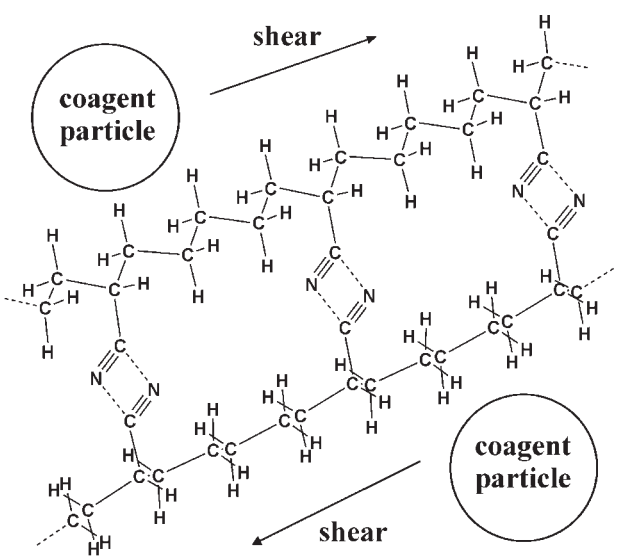

Figure 7 Secondary bonding of the HNBR chains and the hindrance of the latter due to adsorption of the chains onto the ZDMA and TMPTMA particles.

considered to be classical chemical (e.g., peroxide) crosslinking. The elastomer occluded within the voids of primary coagent/filler aggregates,[42] as well as the portion of the elastomer that is adsorbed or otherwise immobilized, is not free to fully share in the microscopic deformation of a coagent/filler and elastomer compound. Because the secondary bond crosslinking is principally determined by the frequency of acrylonitrile groups' encounters,[43] the fraction of occluded elastomer is less likely to translate and therefore form secondary bonds. The HNBR chains before the glass transition remain trapped in a state with little relative mobility, so the effect of bonding is not profoundly exhibited. As the glass transition occurs, the chains gain some mobility and on the one hand tend to orient upon shear and on the other are more likely to form the crosslinks with lengths ranging from 0.472 to 0.494 nm, as the events of individual cyano groups' encounters become more frequent.[43] The crosslinks tend to build up until the temperature at which the formation of the crosslinks upon shear is equilibrated by their dissociation because of the arising molecular motions caused by the elevated temperature. At the temperature of equilibration, the G' maximum is reached, after which HNBR gradually enters the flow. This occurs at lower temperatures for the ZDMA- and TMPTMA-reinforced compounds as the overall number of crosslinks is lower because of the immobilized elastomer, which does not take part in the crosslinking.

HVA-2, however, exhibits plasticizer-like behavior, which can be concluded from the results obtained from DSC and the temperature dependence of G' and tan δ presented in Figure 8. The glass transition shifts toward lower temperatures as the concentration of HVA-2 in the compound is increased. Correspondingly, G' commences to decrease at lower temperatures, and tan δ maxima shift accordingly as well. The apparent G' rise after the rubbery plateau observed for compound 1 diminishes with increasing HVA-2 content. This may be explained either by dilution of the HNBR phase, which forms the secondary bonds responsible for the modulus increase, or by slipping on the HNBR/HVA-2 phase interface. This possibility is favored by the segregated structure of the HNBR/HVA-2 blend and the decrease of tan δ after the glass transition. Overall, probably both processes determine the lowering of the apparent G' value after the rubbery plateau.

For the purpose of modeling the frequency–temperature behavior for compounds 1–7, the dynamic mechanical properties, that is, G' and the loss modulus (G''), were measured in the frequency range of 10^{-2} to 10^{2} Hz while the temperature increased linearly with the constant β value of 1 K/min between −50 and 100°C. It was shown in our previous work[43] that for HNBR samples, the β value of 1 K/min is low enough as the shear dynamics prevail over the dynamics of the ascending temperature in determining the moduli, and this renders the dynamic temperature experiments analogous to isothermal experiments within the experimental error.

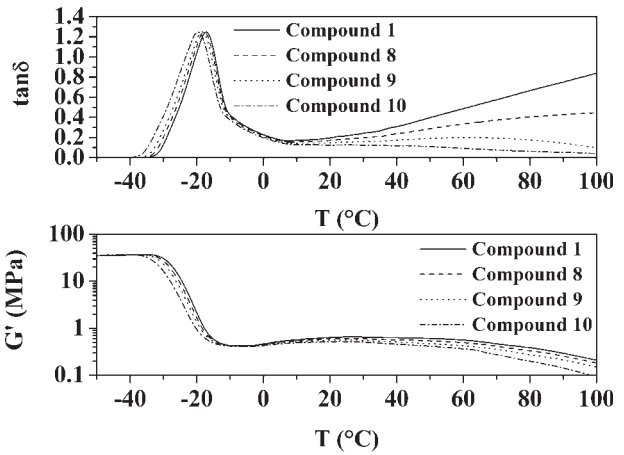

Figure 8 Variation of G' and tan δ with temperature (constant frequency = 1 Hz and β = 1 K/min) for compounds 1, 8, 9, and 10.

The frequency–temperature dependence of the moduli can be expressed with the following equations:[44]

$$\frac{G'(\omega,T)}{\rho(T)T} = \frac{G'(\omega a_T, T_R)}{\rho(T_R)T_R} \tag{2}$$

$$\frac{G''(\omega,T)}{\rho(T)T} = \frac{G''(\omega a_T, T_R)}{\rho(T_R)T_R} \tag{3}$$

where ω is the frequency (rad/s), ρ is the elastomer density, a_T is the shift factor, while T and T_R are the arbrary and the reference temperature. Therefore, to successfully model the frequency–temperature-dependent moduli of the material, a suitable expression for a_T had to be chosen, and G' and G'' at T_R had to be described. The dependence of the elastomer's density on temperature was obtained from our previous work[43] and applied for all compounds as it was observed that the incorporation of the coagents did not noticeably affect the compound density because of the rather small amounts of the coagents added.

The most well known relationship between shift factors and temperature, the WLF equation,[32] still most commonly used for numerous polymers,[45] was used:

$$\log a_T = \frac{-C_1(T - T_R)}{C_2 + T - T_R} \tag{4}$$

The material constants C_1 and C_2 vary from polymer to polymer and can be linked to the Doolittle equation[46] constants. Although frequency–temperature superposition does not necessarily apply to multiphase or semicrystalline polymers,[47] it may generally be successfully performed for uniform and not segregated blends, as was achieved in the case of

ZDMA and TMPTMA, the largest volume portion of the coagent being finely dispersed in the elastomer matrix. The same could not have been expected for the HVA-2 compounds.

The dynamic mechanical properties of HNBR without coagents (compound 1) at T_R were described with the following distribution functions:

$$G'(\omega, T_R) = \int_{\ln\tau=-\infty}^{\ln\tau=\infty} H(\tau)\frac{\omega^2\tau^2}{1+\omega^2\tau^2}\,d\ln\tau \quad (5)$$

$$G''(\omega, T_R) = \int_{\ln\tau=-\infty}^{\ln\tau=\infty} H(\tau)\frac{\omega\tau}{1+\omega^2\tau^2}\,d\ln\tau \quad (6)$$

where $H(\tau)$ is a continuous distribution function at the specific relaxation time (τ). Because the objective of the modeling was not the estimation of the true continuous relaxation spectrum but rather the determination of the dynamic mechanical behavior of the coagent compounds in comparison with the neat HNBR, an arbitrary distribution function was chosen for $H(\tau)$. The stress relaxation modulus for relatively straightforward relaxation processes may be thought to arise from a distribution of relaxation times that is composed of a box and a wedge. This composite, originally suggested by Tobolsky[48] for poly(*iso*-butylene), was generalized as follows:

$$H(\tau) = \begin{cases} M/\tau^n, & \tau_1 < \tau < \tau_2 \\ E_0, & \tau_2 < \tau < \tau_m \end{cases} \quad (7)$$

The distribution embodied in eq. (7) introduces variable parameters M (wedge section proportionality factor), n (wedge section exponent), and E_0 (box section constant modulus) accompanied by integration interval endpoints τ_1 (initial wedge section relaxation time), τ_2 (terminal wedge section and initial box section relaxation time), and τ_m (terminal box section relaxation time). Although the frequency–temperature behavior of neat HNBR (compound 1) can be described with eqs. (2)–(7), the effect of coagents on the dynamic mechanical properties still remains unaccounted. Thavamani and Bhomwick[41] showed that the modified Guth–Gold equation [eq. (8)][49] in the rubbery plateau for various HNBR compounds rather well describes the relation between G' of the neat and reinforced compounds with a temperature-independent effectiveness factor (Ef)[50] of 0.5 for the immobilized occluded elastomer. This was shown even for moderately high amounts of the reinforcing agent:

$$G'(\omega, T)_{\text{reinforced compound}} = \left(1 + 2.5V \text{ 9; } 14.1V^2\right)G'(\omega, T)_{\text{neat elastomer}} \quad (8)$$

where V is the effective volume fraction of the reinforcing coagent. V is determined as follows:

$$V = Ef(\phi + \phi') \quad (9)$$

where ϕ is the volume fraction of the reinforcing coagent and ϕ' is the volume fraction of the reinforcing coagent and immobilized elastomer combined. As the influence of the reinforcing coagent is not the same throughout the entire temperature interval, a temperature-dependent Ef was applied in the model.

The model, consisting of eqs. (2)–(9), was fitted to the experimental G' values for compounds 1–7 and to G'' for compound 1 with the Levenberg–Marquardt algorithm.[51] The T_g determined from the DSC thermogram for compound 1, which is the same as the one determined pycnometrically,[43] was applied as T_R. The $H(\tau)$ parameters were first determined for compound 1, whereas the WLF equation parameters for HNBR were obtained from our previous work.[43] ϕ' was determined from the plateau moduli, with the Ef plateau value of 0.5 being taken into account.[50] The temperature-dependent effectiveness factor for compounds 2–7 was obtained with the proposed equation:

$$Ef = \frac{G'^{RC}_G}{G'_G} - 1 - \left(\frac{G'^{RC}_G}{G'_G} - 1.5\right)\left(1 - \frac{G'(\omega,T) - G'_R}{G'_G - G'_R}\right) \quad (10)$$

where indices G, R, and RC indicate the glassy region, rubbery region, and reinforcing coagent, respectively. Equation (10) encompasses the rather small influence of the reinforcing coagent in the glassy region defined by the ratio $G'^{RC}_G/G'_G - 1$, and it approaches the rubbery plateau value of 0.5[50] by following the behavior of the neat elastomer's frequency- and temperature-dependent G'. The approximation of Ef may of course not be applied for large loadings of the reinforcing agent.

Figure 9 shows that the applied model, consisting of eqs. (2)–(7) for the unfilled compound and of eqs. (2)–(10) for compounds 2–7, relatively well coincides with the experimental results up to a certain temperature, at which the secondary bonding commences to become more distinct. The $H(\tau)$ parameters at sufficiently large τ_m values were found to be 0.122 (n), 3.93 MPa $s^{0.122}$ (M), and 1.13×10^{-2} MPa (E_0) with corresponding integration interval endpoints of 4.30×10^{-3} s (τ_1) and 8.18 s (τ_2). Figure 10 depicts the predicted and experimentally determined G' values in the temperature range of -25 to -20°C and at the applied frequency of 1 Hz. A trend of G' increasing can be observed, regardless of whether ZDMA or TMPTMA was applied in the compound.

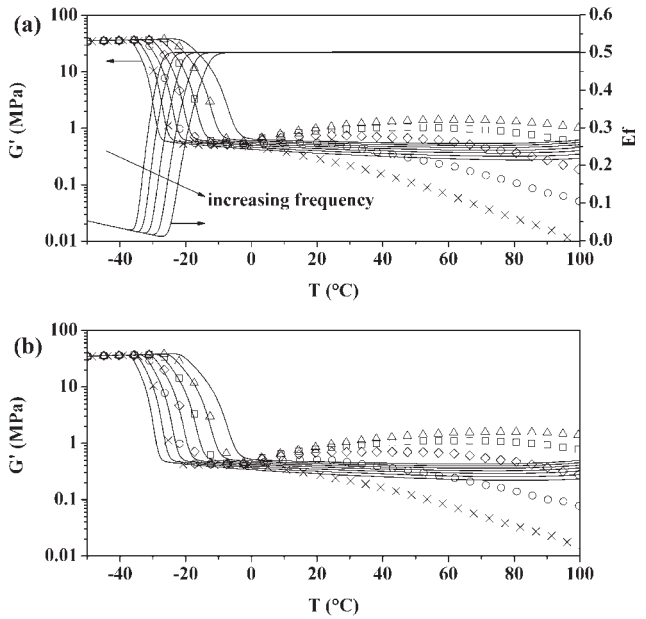

Figure 9 Variation of G' with temperature (constant $\beta = 1$ K/min) for compounds (a) 7 and (b) 1 at frequencies of (△) 100, (□) 10, (◇) 1, (○) 0.1, and (×) 0.01 Hz and the model results, where a_T values were predicted by the WLF equation (—) for the frequency range between 10^{-3} and 10^3 Hz.

Analogously, this can be observed for the amount of the immobilized elastomer calculated from the rubbery plateau moduli, which increase linearly with either the nanophase or microphase volume fraction (Fig. 11). This implies a similar dispersion of the coagent in the rubber matrix for either ZDMA or TMPTMA. Moreover, regarding the dependence of

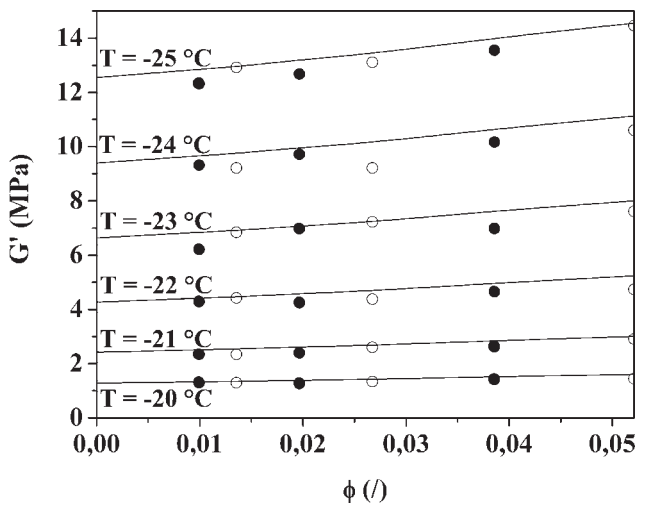

Figure 10 Predicted (—) and experimentally determined [(●) ZDMA and (○) TMPTMA] G' values in the temperature range between −25 and −20°C and at an applied frequency of 1 Hz.

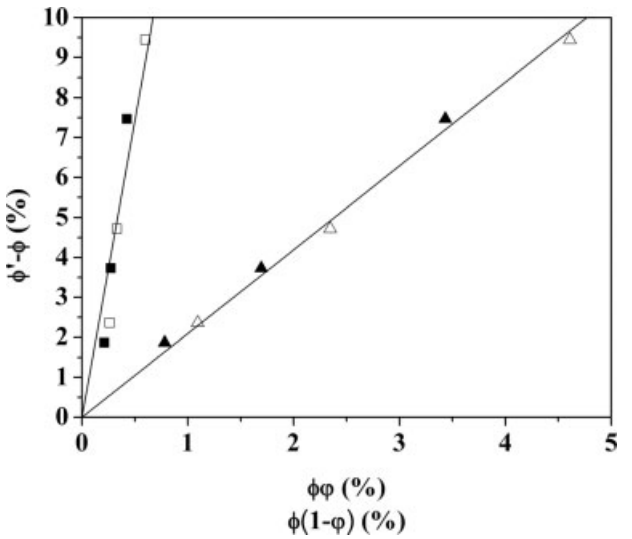

Figure 11 Immobilized elastomer fraction ($\phi' - \phi$) for various fractions of the (▲) ZDMA and (△) TMPTMA nanophases ($\phi\varphi$) and the (■) ZDMA and (□) TMPTMA microphases [$\phi(1 - \varphi)$].

the immobilized elastomer on both the microphase and nanophase fraction, one may come to the conclusion that the nanophase mostly determines the amount of the immobilized elastomer because of its prevalence (Table II) and consequently the relatively large specific elastomer/coagent interface surface, which is principally responsible for the immobilization of the elastomer through the adsorption of its molecules.

The framework of the model can be applied to the crosslinked network, naturally with some reservations. For example, not only will a crosslinked network (e.g., crosslinked HNBR) have different relaxation and dynamic behavior, but the time–temperature (or frequency–temperature) dependence of this behavior also will vary. The same goes for the coagent/filler and the viscoelastic processes inflicted by it, which will of course be dependent on either the elastomer or coagent phase crosslinked structure and, moreover, the interfacial change during the crosslinking process. The model can thus generally be applied if its parameters are newly determined for the system in question (i.e., an elastomer/peroxide/coagent blend after subjection to the vulcanization process at a specific temperature after a certain crosslinking process time). Nonetheless, the combination of a continuous relaxation distribution function, the WLF equation, and the modified Guth–Gold equation seems a reasonable choice for reinforced crosslinked networks as well, should the model parameters be newly determined or at least properly modified to accommodate the viscoelastic behavioral alteration.

CONCLUSIONS

The morphology of blends of coagents ZDMA, HVA-2, and TMPTMA on a reinforcing substrate, DCP, and HNBR after processing was investigated and compared to the results obtained by dynamical mechanical analysis of the blends. APT ^{13}C-NMR spectra confirmed that the coagents did not react in any way during blending.

In ZDMA and TMPTMA blends, both a microphase and a nanophase evolved during processing, whereas the HVA-2 phase in the blends remained well segregated. The volume fraction of the particles under 100 nm in ZDMA and TMPTMA blends was rather large, ranging from 79 to 89%. The ZDMA and TMPTMA particles were more or less spherical because the distributions of equivalent circular and Feret diameters were relatively similar, regardless of the characteristic dimension. A boundary saturation of the elastomer phase with the nanophase was observed, after which the evolution of the microphase became more explicit.

Dynamic mechanical analysis results showed that both ZDMA and TMPTMA exhibited the reinforcing effect during the glass transition and in the rubbery plateau region, whereas HVA-2 exhibited plasticizer-like behavior. Structure ordering through the cyano group secondary bond crosslinking after the rubbery plateau was hindered as the ZDMA and TMPTMA particles were percolated by the HNBR network and the crosslinking around these particles was not possible. In HVA-2 blends, the secondary bond crosslinking was obstructed either by the dilution of the HNBR phase or by slipping on the HNBR/HVA-2 phase interface. Both processes most likely determine the lowering of the apparent G' value after the rubbery plateau.

Dynamic mechanical properties were modeled with the continuous relaxation distribution function, the WLF equation, and the modified Guth–Gold equation. A relationship was proposed for the effectiveness factor, which encompasses the rather small influence of the reinforcing coagent in the glassy region and approaches the average rubbery plateau value of 0.5 by following the behavior of the neat elastomer's frequency- and temperature-dependent G'. The applied model relatively well coincided with the experimental results up to a certain temperature, at which the secondary bonding commenced to become more distinct. The amount of the immobilized elastomer calculated from the rubbery plateau moduli increased linearly with either the nanophase or microphase volume fraction. Moreover, the nanophase probably mostly determined the amount of the immobilized elastomer because of its prevalence and consequently relatively large elastomer/coagent interface.

References

1. Murgic, Z. H.; Jelencic, J.; Murgic, L. Polym Eng Sci 1998, 38, 689.
2. Yanez-Flores, I. G.; Ibarra-Gomez, R.; Rodriguez-Fernandez, O. S.; Gilbert, M. Eur Polym J 2000, 36, 2235.
3. Yu, Q.; Zhou, S. J Polym Sci Part A: Polym Chem 1998, 36, 851.
4. Bucsi, A.; Szocs, F. Macromol Chem Phys 2000, 201, 435.
5. Garcia-Quesada, J. C.; Gilbert, M. J Appl Polym Sci 2000, 77, 2657.
6. Ikeda, T.; Yamada, B.; Tsuji, M.; Sakurai, S. Polym Int 1999, 48, 446.
7. Saethre, B.; Gilbert, M. Polymer 1996, 37, 3379.
8. Saito, Y.; Fujino, A.; Ikeda, A. Jpn. Kokai Tokkyo Koho 136804 (1989).
9. Inoue, T. Prog Polym Sci 1995, 20, 119.
10. Ikeda, T.; Yamada, B. Polym Int 1999, 48, 367.
11. Lu, Y.; Liu, L.; Yang, C.; Tian, M.; Zhang, L. Eur Polym J 2005, 41, 577.
12. Lu, Y.; Liu, L.; Tian, M.; Geng, H.; Zhang, L. Eur Polym J 2005, 41, 589.
13. Samui, A. B.; Dalvi, V. G.; Chandrasekhar, L.; Patri, M.; Chakraborty, B. C. J Appl Polym Sci 2006, 99, 2542.
14. Yuan, X.; Peng, Z.; Zhang, Y.; Zhang, Y. J Appl Polym Sci 2000, 77, 2740.
15. Peng, Z.; Liang, X.; Zhang, Y.; Zhang, Y. J Appl Polym Sci 2002, 84, 1339.
16. Lu, Y.; Liu, L.; Shen, D.; Yang, C.; Zhang, L. Polym Int 2004, 53, 802.
17. Vanaja, A.; Rao, R. M. V. G. K. Eur Polym J 2002, 38, 187.
18. Hopewell, J. L.; George, G. A.; Hill, D. J. T. Polymer 2000, 41, 8231.
19. Hopewell, J. L.; George, G. A.; Hill, D. J. T. Polymer 2000, 41, 8221.
20. Hassan, A.; Wahit, M. U.; Chee, C. Y. Polym Test 2003, 22, 281.
21. Inoue, T.; Suzuki, T. J Appl Polym Sci 1996, 59, 1443.
22. Inoue, T.; Suzuki, T. J Appl Polym Sci 1995, 56, 1113.
23. Ali, Z. I.; Youssef, H. A.; Said, H. M.; Saleh, H. H. Thermochim Acta 2005, 438, 70.
24. Dadbin, S.; Frounchi, M.; Sabet, M. Polym Int 2005, 54, 686.
25. Tai, H. J. Polym Eng Sci 2001, 41, 95.
26. Datta, S. K.; Bhowmick, A. K.; Chaki, T. K.; Majali, A. B.; Despande, R. S. Polymer 1996, 37, 45.
27. Chowdhury, R.; Banerji, M. S. J Appl Polym Sci 2005, 97, 968.
28. Yasin, T.; Ahmed, S.; Yoshii, F.; Makuuchi, K. React Funct Polym 2003, 57, 113.
29. Youssef, H. A.; Ali, Z. I.; Zahran, A. H. Polym Degrad Stab 2001, 74, 213.
30. Jayasuriya, M. M.; Makuuchi, K.; Yoshi, F. Eur Polym J 2001, 37, 93.
31. Banik, I.; Dutta, S. K.; Chaki, T. K.; Bhowmick, A. K. Polymer 1999, 40, 447.
32. Williams, M. L.; Landel, R. F.; Ferry, J. D. J Am Chem Soc 1955, 77, 3701.
33. (a) Vogel, H. Phys Z 1921, 22, 645; (b) Fulcher, G. S. J Am Ceram Soc 1925, 8, 339; (c) Tammann, G.; Hesse, W. Z Anorg Allg Chem 1926, 156, 245.
34. Ding, Y.; Sokolov, A. P. Macromolecules 2006, 39, 3322.
35. Liu, C. Y.; Halasa, A. F.; Keunings, R.; Bailly, C. Macromolecules 2006, 39, 7415.
36. Liu, C. Y.; He, J.; Keunings, R.; Bailly, C. Macromolecules 2006, 39, 8867.
37. Dixon, K. W. In Polymer Handbook; Bandrup, J.; Immergut, E. H.; Grulke, E. A., Eds; Wiley: New York, 1999; Chapter 2.

38. Van Berkel, P. M.; Punt, M.; Koolhaas, G. J. A. A.; Driessen, W. L.; Reedijk, J.; Sherrington, D. C. React Funct Polym 1997, 32, 139.
39. Grenier-Loustalot, M. F.; Da Cunha, L. Polymer 1997, 38, 6303.
40. Liu, L.; Luo, Y.; Jia, D.; Guo, B. Int Polym Proc 2004, 19, 374.
41. Thavamani, P.; Bhomwick, A. K. J Mater Sci 1992, 27, 3243.
42. Medalia, A. I.; Kraus, G. In Science and Technology of Rubber; Mark, J. E.; Erman, B.; Eirich, F. R., Eds.; Academic: San Diego, 1994; Chapter 8.
43. Likozar, B.; Krajnc, M. e-Polymers 2007, 131, 1.
44. Plazek, D. J. J Phys Chem 1965, 69, 3480.
45. Ferry, J. D. Viscoelastic Properties of Polymers; Wiley: New York, 1980.
46. Doolittle, A. K.; Doolittle, D. B. J Appl Phys 1957, 28, 901.
47. Shaw, M. T.; MacKnight, W. J. Introduction to Polymer Viscoelasticity; Wiley: Hoboken, NJ, 2005.
48. Tobolsky, A. V. Properties and Structure of Polymers; Wiley: New York, 1960.
49. Medalia, A. I. Rubber Chem Technol 1973, 46, 877.
50. Medalia, A. I. Rubber Chem Technol 1972, 45, 1172.
51. Marquardt, D. SIAM J Appl Math 1963, 11, 431.